
ACOUSTIC SIGNAL PROCESSING.
COMPUTER SIMULATION

Tomographic Estimation of Waterbody Parameters in the Presence of Ice Cover Using Seismoacoustic Sources

D. A. Presnov^{a, *}, A. L. Sobisevich^a, P. D. Gruzdev^b, V. I. Ignatiev^c, A. I. Kon'kov^d, A. Yu. Moreev^b,
A. V. Tarasov^{c, d}, A. A. Shuvalov^{c, d}, and A. S. Shurup^{a, e}

^a*Schmidt Institute of Physics of the Earth, Russian Academy of Sciences, Moscow, 123242 Russia*

^b*JSC Concern MPO-Gidropribor, St. Petersburg, 194044 Russia*

^c*LLC GEODEVICE, St. Petersburg, 199406 Russia*

^d*St. Petersburg State University, Department of Physics, St. Petersburg, 199034 Russia*

^e*Moscow State University, Department of Physics, Moscow, 119991 Russia*

**e-mail: presnov@physics.msu.ru*

Received April 29, 2019; revised May 6, 2019; accepted May 7, 2019

Abstract—The article presents the results of field tests of marine seismic sources and seismoacoustic areal measuring systems based on autonomous embedded buoys in Lake Ladoga under ice conditions. The authors demonstrate the possibility of separating in the received signal individual modes propagating in the ice cover–water layer–sediment layer–elastic half-space system. An iterative tomographic scheme is proposed that makes it possible to reconstruct high-contrast high-speed anomalies in the considered layered medium. The results of tomographic estimation of the bottom, water layer, and ice layer characteristics in the active mode are presented.

Keywords: seismic tomography, electric sparker, layered medium, normal waves, joint estimation of the acoustic ice, water, and bottom characteristics

DOI: 10.1134/S106377101905018X

INTRODUCTION

Since the second half of the 20th century, applied problems in studying the geological structure and oceanographic conditions of the Arctic shelf have steadily played an increasing role. The main specific feature of the Arctic shelf is the presence of continuous ice cover, which limits the use of vessels in various types of research. A natural solution may be to embed scientific equipment directly in the ice cover. A promising method for studying the physical characteristics of the environment is tomography with placement of receivers at the boundary or throughout a given region; this method is successfully being developed today for studying inhomogeneities in the ocean [1] and geological structures of the solid Earth [2]. An advantage of this approach is remote study even in areas of the environment where it is impossible to install equipment for contact measurements. The aim of this study is an in situ test of the developed seismoacoustic tomography method [3], taking into account the features of signal reception and emission governed by the presence of ice cover.

It should be noted that in the absence of ice cover, there has been considerable success in experimentally separating hydroacoustic modes of various numbers,

reconstructing currents, and determining the parameters of seafloor surface layers [4–7]. However, due to the significant temporal instability of the ocean, as a rule, complex signals and expensive sources are used. The theoretical background for processing hydroacoustic signals in an Arctic waveguide is described in [8] and references therein. One of the first experiments to measure the travel time of various modes in ice conditions was attempted in [9] using standard seismic and hydroacoustic equipment. In this study, active seismoacoustic tomography was tested with specialized autonomous geohydroacoustic buoys [10] developed at the Institute of Physics of the Earth of the Russian Academy of Sciences, as well as pulsed seismic sources.

It was shown earlier [11] that the total wave field in a medium with ice cover, a water layer, and elastic half-space includes several mode components that make the main contribution to the low-frequency region: the flexural-gravity wave of the ice cover, the Rayleigh-type bottom surface wave, and hydroacoustic mode signals. It is important that these waves differ from each other both in frequency and propagation velocity [11]; i.e., they can be separated by time-frequency analysis of the seismoacoustic field recorded in a sufficiently wide frequency band using spaced

seismoacoustic receivers. Numerical study of the influence of variations in the model's parameters on perturbations in the propagation time of mode signals demonstrated [11] the possibility of separate tomographic reconstruction of the characteristics of the studied medium by separately considering the flexural wave of the ice cover (depending on the ice parameters), hydroacoustic modes (making it possible to estimate the water layer characteristics), as well as the fundamental mode of the Rayleigh-type surface wave (which carries information about the properties of the elastic half-space). Earlier, it was also demonstrated experimentally [3, 9, 16] that the propagation times of the above-mentioned mode signals can be estimated using only seismic receivers located on the ice surface. This greatly simplifies full-scale experiments, since they do not require seismoacoustic receivers either on the bottom or in the water column. The previously obtained theoretical results [11], as well as the first data of field measurements [3, 9, 16], allow more detailed consideration of the problem of joint tomographic reconstruction of the physical properties of the ice cover, bottom sediments, and the water layer based on the experimental reception of various modes carrying information on the propagation medium in the ice cover–water layer–sediment layer–elastic half-space model.

In order to solve the problems in this study, at the beginning of April 2018, an expedition was conducted at the Ladoga hydroacoustic test site of the Karelian Branch of JSC Concern Oceanpribor. The site is in the northwestern part of Lake Ladoga in Naysmeri Bay and is a fjord elongated for several kilometers, about 350 m wide. The remoteness of the site from industrial facilities and shipping lanes ensures low acoustic noise at the level of natural noise. At the same time, the site has a suitable coastal infrastructure for various types of research.

In April 2018, the weather at the site was quite favorable, the temperature during the daytime remained around 0°C and reached –6°C at night, and a calm northeast wind blew in open areas. The ice cover was coated with a thin (about 2–5 cm) layer of snow; the thickness of ice was in different places from 20 to 35 cm. Measuring points were arranged on the surface of the ice cover at the vertices of a regular pentagon, and the source was located near the coast. Spring is not always a propitious time for ice expeditions due to recurring transition of the ambient temperature through 0°C, which can form water layers in the ice stratum that prevent accurate embedding of instruments.

HARDWARE SYSTEMS

Today, when studying the structure of the upper part of bottom sediments (up to 100 m), various sources are used to solve engineering problems in water areas, the main ones being are sonars, small seis-

mic gun, and electric sparkers [12]. It is precisely sparkers that have a number of competitive advantages, which include the ability to quickly change the shape, intensity, and spectral content of the pulse; the absence of steam vapor pulsations; and the ability to create a given directivity pattern via the grouping of sources.

In the present study, a single sparker was used to excite a high-frequency acoustic pulse in performing high-resolution seismic borehole surveys. The operating principle of the sparker (Fig. 2a, top right) is the creation of electric breakdown between groups of electrodes, causing a spark. The main technical element of the sparker is the energy storage unit, which completely governs all the acoustic parameters of the excited signal. We used a sparker and energy storage unit manufactured by LLC GEODEVICE—the MultiJack 500HP1.5 (Fig. 2a)—which yields a pulse energy of ~500 J.

For seismoacoustic signal reception on the ice surface, autonomous embedded buoys were used [10], including a molecular electronic broadband sensing element, a recorder with a precise time synchronization system, and a battery pack. Such systems can be quickly placed in an ice field by a single person. Where possible, a hole was cut in the ice to a depth of about 25 cm, into which the ice system module was lowered on a sand cushion. To protect against wind noise, installation spot was covered with snow. As part of the experiment, the vertical vibrational velocity component was measured by buoys in the frequency range from 0.03 to 50 Hz. Figure 1 shows the positions of the receiving points (triangles with the base below) with respect to the shores and topography of the bottom of the waterbody, and the emission point (the triangle with the base above). The receiving system worked autonomously for 5 days. Additionally, we used piezoceramic control hydrophones installed at half the depth of the waterbody, 20 m northwest of the source, as well as a CM3-OS type low-frequency vertical pendulum seismometer (sensitive to changes in vibrational velocity) installed on a massive concrete block on the shore 20 m north of the source's location. Data from additional instruments were received on a Reftek-130B seismic recorder and recorded at a digitization rate of 1 kHz.

The sparker was lowered from a surface vessel, which provided power, to a depth equal to half that of the waterbody; it emitted signals with a periodicity of 10 s. The stationary conditions of the experiment allowed us to detect, in the course of processing, 12 identical signals, which were coherently added to reduce the effect of background noise. Figure 3 shows the waveforms of an acoustic pressure pulse propagating in water (Fig. 3a) and transforming as it passed the coastal wedge into a seismoacoustic perturbation on the coast (Fig. 3b). The channels are synchronized, but the time scale on the graphs differs. The signal

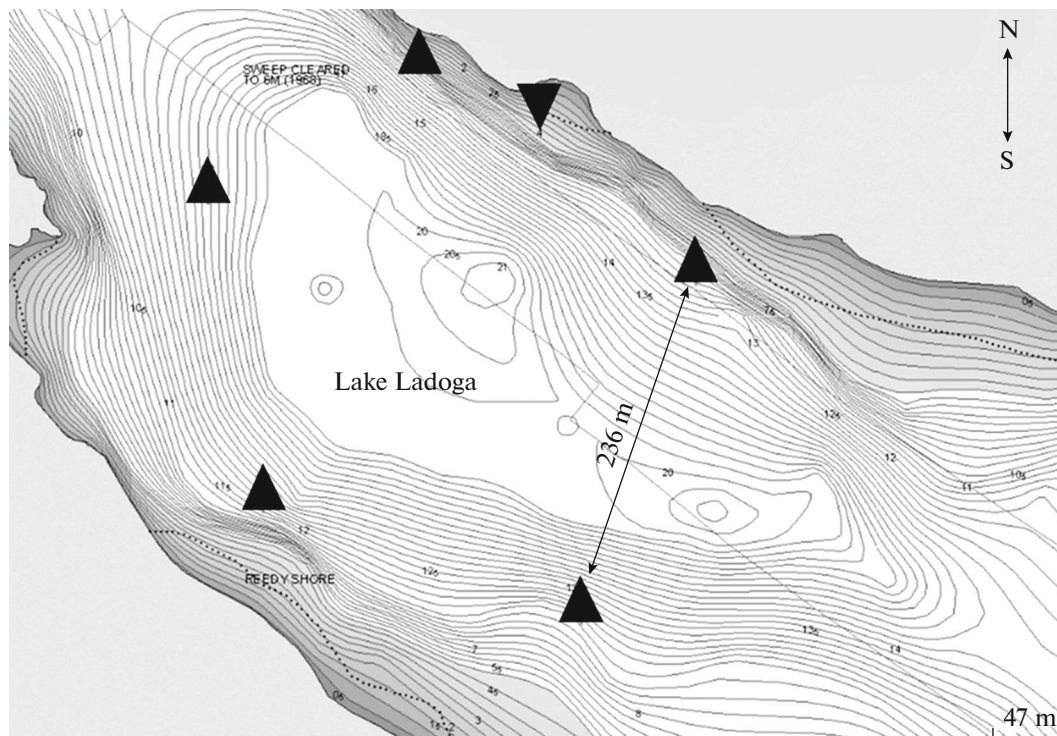


Fig. 1. Scheme of experimental work on Lake Ladoga. Regular triangles are reception points. Inverted triangle is emission point. Bathymetry is shown by contour lines.

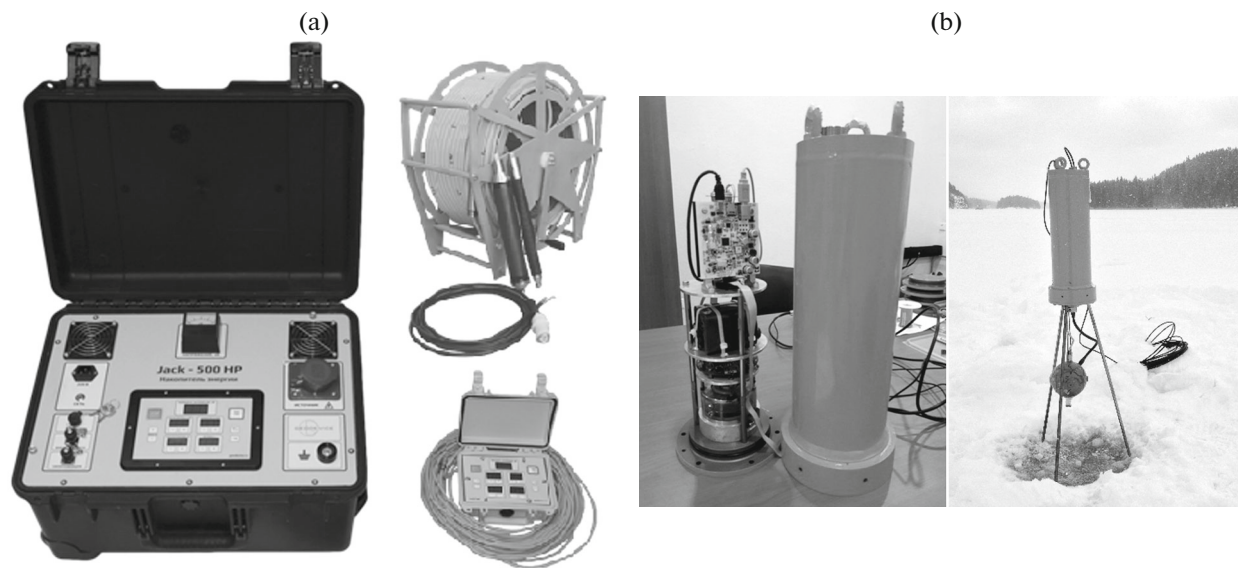


Fig. 2. Hardware used: (a) sparker with energy storage unit; (b) ice-class geohydroacoustic measuring buoy.

from the sparker is observed against high-amplitude low-frequency noise interference with the characteristic period of microseismic oscillations. However, the good repeatability of the generated pulse allows it to be accurately detected, even with a low initial signal-to-noise ratio (Fig. 3b). In particular, the coherent addition of signals recorded by the seismic receiver

increased the signal-to-noise ratio by 23 dB. The structure of the signal recorded by the hydrophone (Fig. 3a) is ambiguous due to the formation of a complex interference pattern due to multiple reflections from bottom sedimentary layers, ice cover, the coast, and the sides of the ship. The short signal duration is noteworthy, only a few tens of milliseconds. It can also

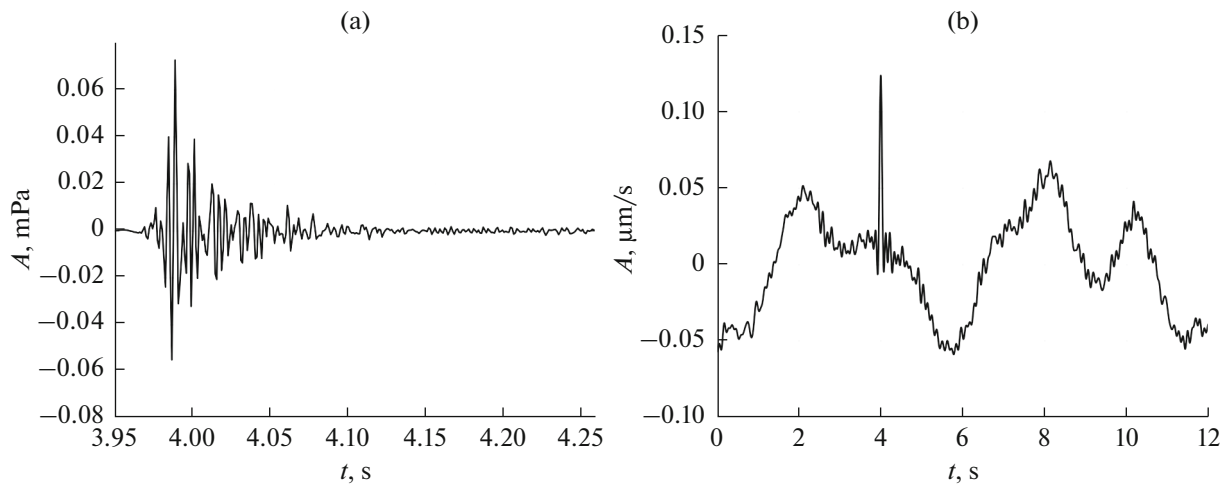


Fig. 3. Pulse generated by sparker at half of waterbody depth, recorded by hydrophone in frequency range (a) 50–500 Hz and (b) seismic receiver in frequency range of 0.03–10 Hz on coast.

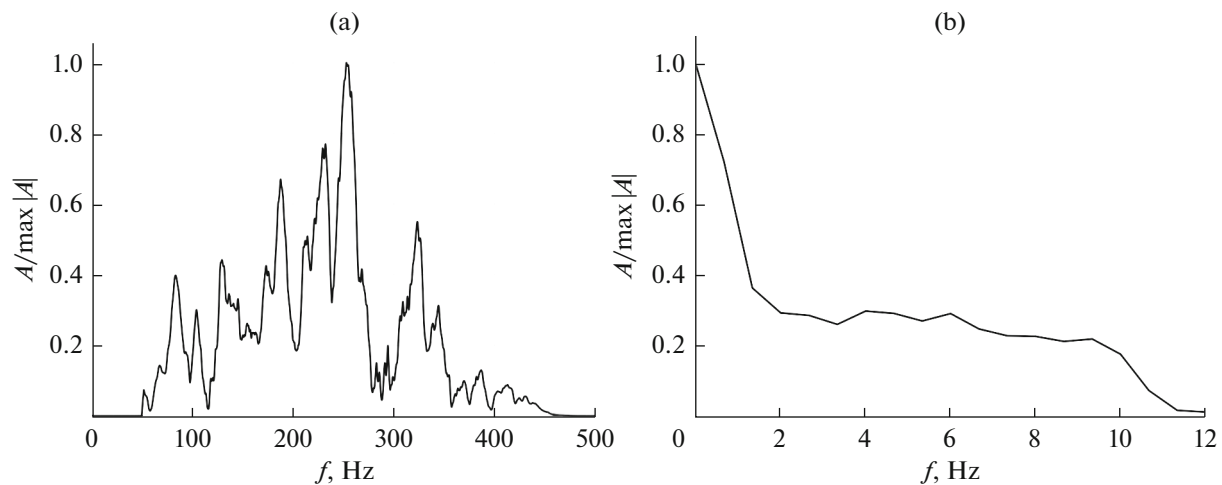


Fig. 4. Normalized amplitude spectrum of sparker signal recorded by (a) hydrophone in the water layer and (b) seismometer on shore, at about the same distance from the source as the hydrophone.

be seen that the acoustic pressure amplitude in water is large enough to accurately distinguish it from the background noise.

Figure 4 shows the frequency content of the acoustic pressure pulse generated in the water layer (Fig. 3a). The amplitude spectrum has an oscillating character with a maximum in the vicinity of 250 Hz. An important feature of the sparker is the dependence of the spectral content of the excited pulse on its intensity. With allowance for the features of the receiving equipment, the low-frequency signal was recorded only on shore (Fig. 4b). Meanwhile, the presence of the signal in the entire frequency range is noteworthy.

Thus, the energy storage unit and the sparker are high-quality instruments that can generate sufficiently broadband high-amplitude acoustic pressure pulses. An important feature is the good repeatability of sig-

nals, allowing them to coherently accumulate, which increases the signal-to-noise ratio in the low-frequency region. However, far from the coastline, the use of this type of source may be complicated due to increased power supply requirements.

The ice-embedded receiving system used in this work is low-frequency, which prevents its use with a sparker. For this reason, to implement the tomographic measurement scheme, we used an seismic gun manufactured by GEODEVICE. The seismic gun fired a series of shots with a power of 2.7 kJ as close as possible to the lakebed surface. Recording was carried out on the surface of the ice cover with embedded geohydroacoustic buoys. As an example, Fig. 5 shows the signal recorded at a distance of 165 m from the source, as well as its spectrum. It can be concluded that for solving the problems of the present study, the seismic

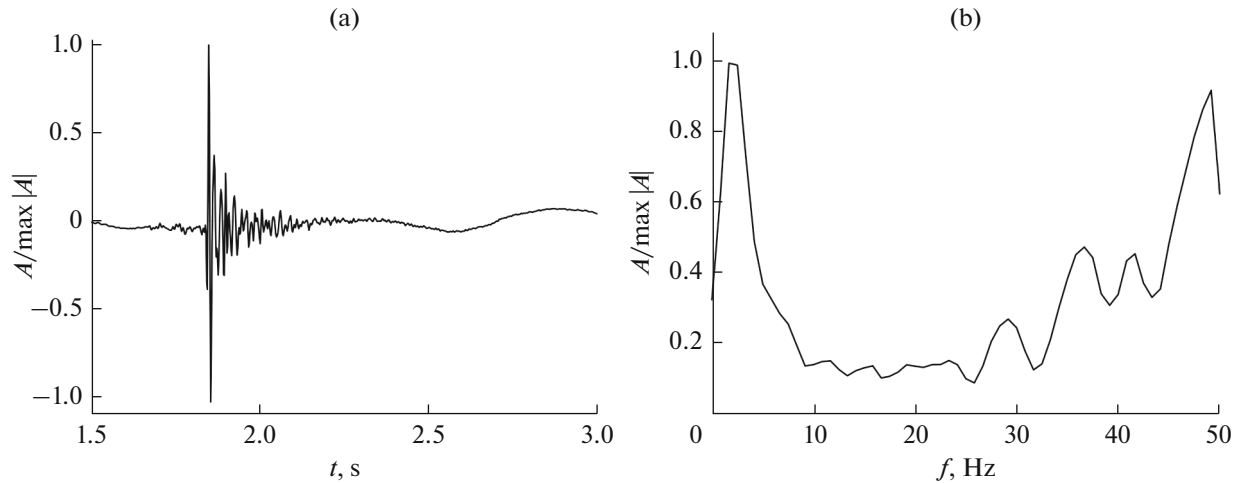


Fig. 5. Seismoacoustic signal from shooting of blank cartridge near bottom recorded (a) on ice surface and (b) its amplitude spectrum.

gun is preferred, since it can excite pulses in the required frequency range and is much more mobile.

SEPARATION OF MODE COMPONENTS OF SEISMOACOUSTIC FIELD

The first stage of tomographic research is to construct a background model of the medium that approximately satisfies the experimental conditions and allows theoretical calculation of the kinematic parameters of expected seismoacoustic signals. As seen in Fig. 1, the lake depth at the measuring sensor installation sites varies from 13 to 20 m. A study of the literature data revealed that the bottom in Naysmeri Bay is covered with a silt layer up to 18 m thick and the underlying rocks consist of rapakivi granites. This made it possible, as an initial approximation, to propose a layered model of the medium whose parameters are longitudinal wave velocity c_l , transverse wave velocity c_t , density ρ and layer thickness h listed in Table 1. A distinctive feature of the model is the presence of a soft sediment layer.

The results of [11] were used to calculate in the model of the medium the phase c and group v velocities of the seismoacoustic modes formed in an ice-covered medium. The calculation results showed that the wave field in the low-frequency region is the sum of a sufficiently large number of mode components. Below, we confine ourselves to considering only the flexural-gravity wave of the ice cover, the fundamental mode of a Rayleigh-type surface wave, and the first normal hydroacoustic mode (Fig. 6, the considered portions of the dispersion curves are shaded grayed), which in the experimental conditions made the main contribution to the recorded low-frequency wave field.

As noted above, in Fig. 1 shows the placement of the embedded geohydroacoustic buoys. Near each measurement point at the bottom, the seismic gun

fired several signals successively. As a result, 20 paths along which the wave disturbance propagates were obtained. The experimental conditions and, in particular, the density of the ice cover, prevented ideal distances between points, so the actual distances vary from 165 to 372 m. The lake depth at the location points was on average 13 m. In Fig. 6, gray shading indicates mode components in the frequency range recommended for the experiment in view of the high signal-to-noise ratio. This frequency range is limited from below near $f=6$ Hz, where the speeds of the fundamental and bending modes have close values, and, therefore, it is not difficult to separate them in the received signal. The situation is also complicated by the presence of low-frequency noise at frequencies below 10 Hz.

To determine travel times τ signals along different paths, the cross-correlation function was calculated $K(\tau)$ between the signal recorded at the point of emission and the signal received at a remote location. It was assumed that the propagation medium is isotropic, and for each pair of measuring points, the cross-correlation functions of signals emitted from opposite sides were averaged. Filtering in various frequency ranges by the position of the maximum envelope of the cross-correlation function makes it possible to determine the travel time of various frequency components of the emitted signal. Following the results of numerical calculation presented in Fig. 6, we note that the

Table 1. Parameters of initial layered medium model

	h, m	$c_l, km/s$	$c_t, km/s$	$\rho, kg/m^3$
Ice	0.2	2.2	1.7	900
Fluid	20	1.5	—	997
Sediment	18	0.7	0.4	2000
Base	—	4.5	2.7	2600

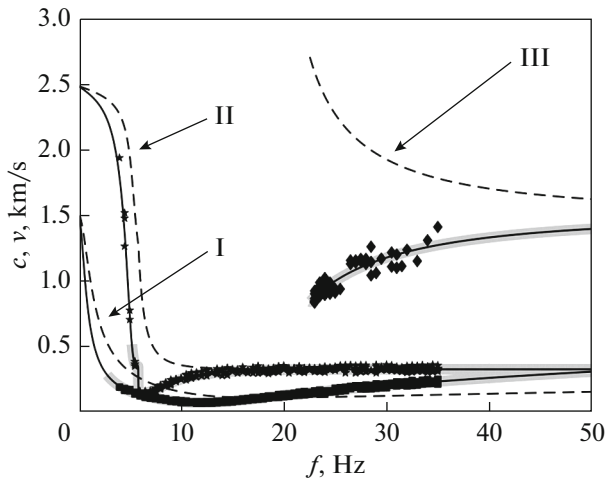


Fig. 6. Dispersion curves of seismoacoustic modes of lowest numbers formed in model of medium with parameters specified in Table 1. I, flexural-gravity wave; II, fundamental mode of Rayleigh-type surface wave; III, first normal hydroacoustic mode. Solid lines, group velocities v ; dotted lines, phase velocities c . Dots mark velocity estimates obtained in experiment.

nontrivial problem of mode separation using single receiving stations in the general case can be solved with indicated model of the medium, since the considered modes have different propagation velocities in the given frequency range. Thus, the shortest travel time will be at the first normal hydroacoustic wave, then the Rayleigh-type surface wave arrives, and finally, the flexural-gravity wave. Moreover, in the low-frequency region (up to 23 Hz), the correlation function should have only two maxima, since hydroacoustic modes do not propagate at these frequencies. To determine the reliable maxima of the envelope of

the cross-correlation function, they were sought in a 20% interval of the travel times calculated from the model group velocities (Fig. 6). As an example, Fig. 7 shows the cross-correlation functions of signals propagating along a path 236 m in length (see Fig. 1) for two frequency ranges 5.8–8.2 Hz (Fig. 7a) and 29.9–35.1 Hz (Fig. 7b). The positions of the maxima that meet the above condition are plotted in gray on the graph. As a result, the experimental travel times along various tracks in several frequency ranges were estimated. The points in Fig. 6 plot the travel times, calculated from the experimental estimates, along a straight line. These results will be used below in the tomographic estimation of the ambient parameters.

TOMOGRAPHIC SCHEME

To solve the inverse problem, we employ the linearized tomographic scheme proposed earlier in [13, 14] and used to reconstruct the characteristics of the water layer [13], as well as the bottom parameters [14]. In the present studies, the authors have attempted to generalize the results obtained in the case of joint reconstruction of the ice, water layer, and bottom parameters. As in [13], the desired two-dimensional velocity distribution in the medium was decomposed into basis functions forming a banded basis. The perturbation matrix represents the delay of the propagation times of mode signals with respect to the background velocity model of the medium, caused by sequential introduction of the model parameters requiring reconstruction into each of the basic perturbation bands. Assuming that the perturbations of the mode propagation times observed in the experiment can be represented as a linear combination of time delays caused by basis functions, the solution of the inverse problem of reconstructing spatial distributions

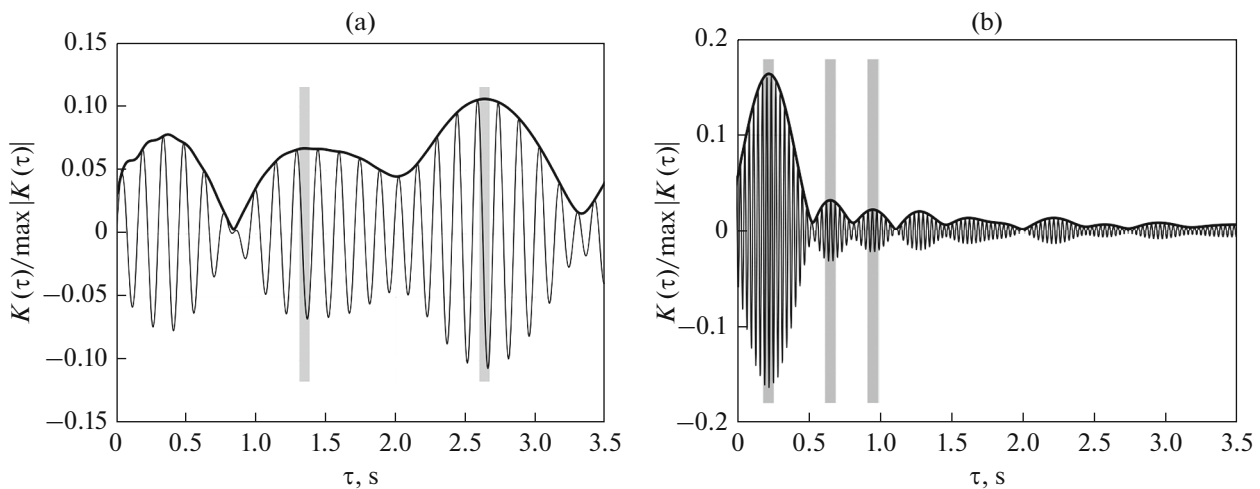


Fig. 7. Example of estimating propagation times of various signal mode components based on narrowband filtering of cross-correlation function. (a) Center frequency $f = 7$ Hz, bottom surface, and bending modes; (b) center frequency $f = 32.5$ Hz, hydroacoustic, bottom surface, and bending modes.

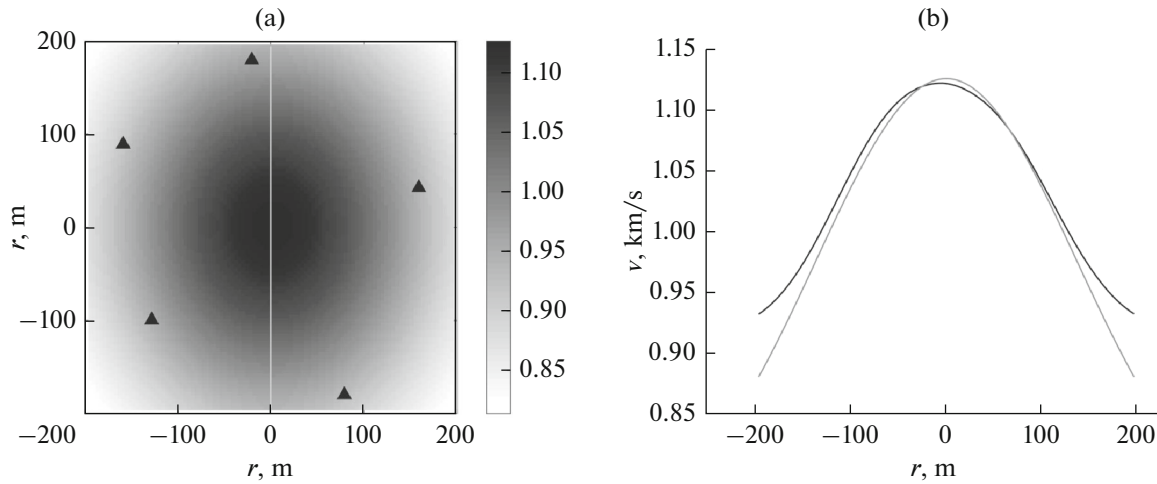


Fig. 8. (a) Specified distribution of group velocity of first normal hydroacoustic mode at frequency $f = 27$ Hz with contrast of 30%; (b) section (a) passing through zero of abscissa axis: given model (gray), result of tomographic reconstruction (black).

of environmental parameters can be reduced to solving a system of linear equations for the unknown coefficients of expansion of these parameters over a banded basis. The process of constructing perturbation matrices using banded type for the joint reconstruction of various parameters of the medium is described in detail in [1, 13, 14].

At the first stage, in order to assess the capabilities and limitations of the approach, in measurement conditions, numerical simulation was performed with parameters close to the experimental conditions. In accordance with the results of [14], the three-dimensional problem was divided into two two-dimensional ones. In this case, at each point of the horizontal plane, the medium was vertically layered. To describe the region (Fig. 1), a square grid with a step of 5 m was constructed on a 500×500 m area. At each grid node, the medium was a layered model: an elastic half-space, elastic sedimentary layer, fluid layer, and elastic ice cover layer.

As shown in [15], the wave field in the layered model can be represented as the sum of individual mode components having different propagation velocities. To calculate the phase and group velocities, the dispersion equation was solved numerically. In this case, following the results of [11], the thickness of the water layer, the velocity of transverse waves in the sedimentary layer, and the thickness of the ice cover will have the greatest influence on the velocities of the considered modes. In the horizontal plane, we specified perturbation of the parameters of the medium in the form of a two-dimensional axisymmetric Gaussian function. Taking into account the bottom topography data (Fig. 1), the model parameters given in Table 1 were chosen as the initial parameters; their perturbation at the maximum of the Gaussian function reached 30% that of the background values. As a result, the horizontal distribution of the group veloci-

ties v of different modes at different frequencies f was calculated. As an example, Fig. 8 shows the calculated distribution of the model group velocity v of the first normal hydroacoustic mode at a frequency $f = 27$ Hz when the depth of the fluid layer varies from 15 to 20 m, which corresponds to the experimental conditions. The propagation times of signals between all pairs of sources and receivers for given spatial distributions of the group velocities of modes were calculated in the ray approximation by numerically solving the eikonal equation [14], which made it possible to obtain “experimental” data for solving the inverse problem. The obtained times were then used to study the stability of the solution to the inverse problem with the addition of random noise to the initial data for a given amount and configuration of the basis functions, as well as to estimate the resolution of the tomographic scheme. The standard method was used to calculate the discrepancy of the obtained solution:

$$\eta_r = \sqrt{\frac{\sum_{i,j} |T_i - \hat{T}_i|^2}{\sum_{i,j} |T_i|^2}},$$

where T_i the travel time of the experimental signal between the i th pair and \hat{T}_i the signal travel time between the i th pair, calculated theoretically in the ray approximation for the reconstructed model of the medium.

A sufficiently strong velocity contrast (Fig. 8a) can lead to deviation from the linear approximation when solving the inverse problem, which required an iterative approach to obtain estimates of the medium with acceptable accuracy. In this case, at each iterative step, the correction to the velocity distribution in the medium with respect to the velocity model obtained at the previous step is reconstructed. At the first iteration, a uniform distribution was taken in accordance with the parameters specified in Table 1. A satisfactory

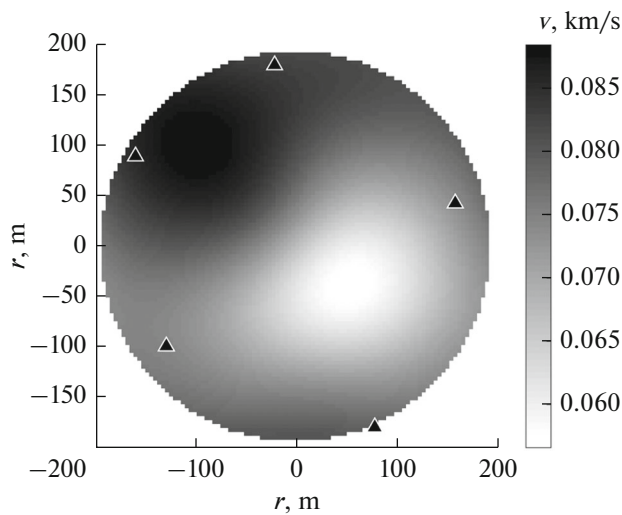


Fig. 9. Result of tomographic reconstruction of distribution of group velocity of flexural wave of ice cover at frequency $f = 9.5$ Hz.

result of solving the inverse problem using model data was obtained after five iterations for all three considered modes with different velocities. As an example, Fig. 8b shows the reconstructed and given value of the group velocity of the first normal hydroacoustic mode at frequency $f = 27$ Hz in the section of the original model shaded gray in Fig. 8a. The discrepancy of the right side was $\eta_T = 0.009$; the discrepancy of the solution (calculated similarly η_T , see [14]) was $\eta_{\Delta v} = 0.03$. The simulation showed that when used in the decomposition of four basis bands rotated at seven angles, the resolution obtained using the considered configuration of the receiving system does not exceed 100 m. An increase in the number of basis functions leads to an increase in resolution, but also to deterioration in the condition of the disturbance matrix for a fixed amount of source data, which requires greater regularization of the solution and leads to an increase in the discrepancy of the solution. Adding random noise to the initial data with zero mean and root-mean-square amplitude deviation, which is 1–5% of the mean-square value of the initial data, did not lead to a significant deterioration in the reconstruction results. The random perturbations in the reconstruction results observed in this case were smoothed after spatial filtering of the resulting estimates.

The selected parameters for solving the inverse problem (basis, regularization, and filtering parameters) determined by numerical simulation were used at the next stage for inversion of the experimentally estimated propagation times. At this stage of the study, tomographic reconstruction of the group velocities of the wave modes for individual frequency ranges was performed.

We begin our consideration with a slow flexural-gravity mode, the energy of which is concentrated near the ice cover. Figure 9a shows the result of reconstructing the distribution of the group velocity of a flexural wave near frequency $f = 9.5$ Hz after three iterations; the discrepancy was $\eta_T = 0.06$. The velocity of this wave is mainly determined by the thickness of the ice cover, while lower speeds (light colors) correspond to thinner ice. The result obtained is generally consistent with the observations of the expedition participants; in the southeastern region, the ice cover was extremely heterogeneous and consisted of alternating layers of solid ice, fluid, and snow. In particular, this led to displacement of the receivers with respect to the originally planned observation scheme with an equilateral pentagon. In the northwestern part, the lake is deeper and the ice was consolidated. The velocity values on the brightness scale in Fig. 9 can be conditionally converted to an ice thickness scale with a range of 5–40 cm (in the general case, the elastic properties of the ice cover should be taken into account).

Figure 10 shows the reconstructed velocity distribution of the fundamental mode of the Rayleigh-type surface wave at a center frequency of 28.5 Hz, the velocity of which depends in a complex manner on the sediment characteristics. The discrepancy after four iterations was $\eta_T = 0.09$. Taking into account the rough relationship between the penetration depth and the length of the surface-type wave, the obtained distribution can be attributed to the sedimentary layer at a depth of 7 m. The bottom of the lake in the study area has subsided. It can be assumed that low-velocity sediment accumulates in this depression, which leads to the fact that the velocities on its slopes are higher. It is noteworthy that the solution to the inverse problem did not take into account the rather complex bottom topography, which may lead to velocities in the reconstruction results due to the increase in the geometric path traveled by the wave.

Figure 11 shows the reconstructed velocity distribution of the first normal hydroacoustic mode, which characterizes the parameters of the water column. After five iterations, the discrepancy is $\eta_T = 0.04$. Given the weak resolution of the receiving system, we note that the velocity of the hydroacoustic mode is maximum in areas of the medium where the depth of the lake is greater. Thus, under the experimental conditions, the nature of the depth dependences of the velocity of the surface wave and the hydroacoustic mode are opposite.

Based on the data obtained, it can be concluded that the initial parameters of the model of the medium in Table 1 vary quite strongly in the horizontal plane. In particular, variations in the thickness of the ice cover reach 100% with respect to the background. The ice has a complex structure, because the experiment was carried out in spring, when the ice began to melt repeatedly. Using the approximate relationship

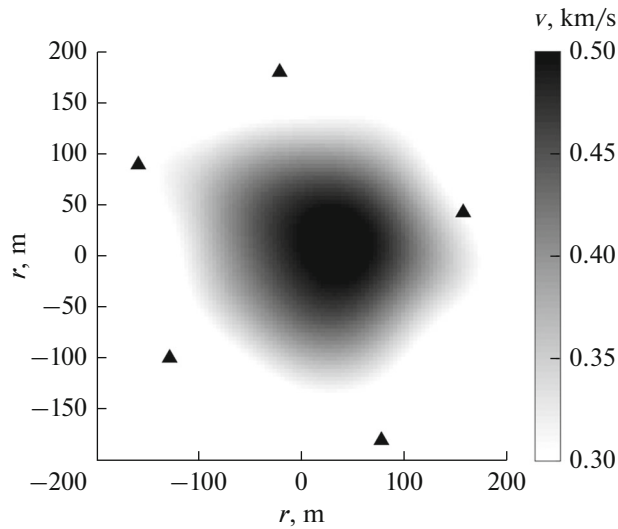


Fig. 10. Result of tomographic reconstruction of group velocity distribution of fundamental mode of bottom surface wave at frequency $f = 28.5$ Hz.

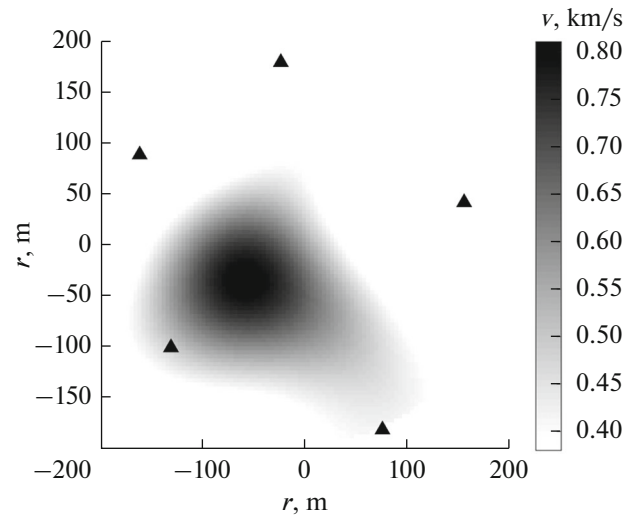


Fig. 11. Result of tomographic reconstruction of group velocity distribution of first normal hydroacoustic mode at frequency $f = 33$ Hz.

between the velocity of the Rayleigh-type wave and the velocity of transverse waves $v = 0.9c_s$, we note that variations in the velocity of transverse waves in sediments are in the range of 0.27–0.45 km/s, which correspond to fairly soft geological structures such as clayey soils. Analyzing the distribution of the group velocity of the hydroacoustic mode in the absence of currents and other scatterers in the water column, it can be concluded that the changes in velocities are associated only with the change in depth of the waterbody, which accordingly reaches 30% with respect to the value in Table 1.

CONCLUSIONS

Domestic modern borehole and marine seismic sources have been tested in situ. Processed experimental data were used to analyze the spectral content of seismoacoustic signals excited by a sparker and seismic gun in the water column under ice cover. The high stability of the generated pulses was confirmed, which makes it possible to successfully use sources for solving seismic engineering tasks in shallow water.

Operations with the developed embedded autonomous geohydroacoustic buoys revealed that the most intense background noise recorded on ice lies in a frequency range not exceeding 10 Hz, which is significantly lower than the center frequency of the sparker. This makes it possible to use the marine modification of the reflected wave method to study the upper part of the profile in ice-covered waters.

The authors proposed and experimentally tested an active tomographic scheme for joint estimation of the ice cover, water layer, and bottom sediment parameters with the aid of specialized receivers embedded on

the ice at the boundary of the studied area. An iterative algorithm was used to reconstruct strongly contrasting inhomogeneities. The discussed approach is based on the possibility of separating the individual mode components of signals in the experimental data and estimating their time delays caused by the presence of reconstructed inhomogeneities. As a result of processing field measurement data, it was possible to isolate various modes of the wave field that formed in the ice conditions of the experiment. For mode signals, which make the main contribution to the recorded field, group velocity maps of the studied area were reconstructed in various frequency ranges, along the perimeter of which the receivers were located. The results suggest that it is possible to jointly reconstruct the bottom, water column, and ice cover characteristics with respect to the propagation times of individual mode signals recorded by seismic receivers located on the ice surface. The next stage of research proposes to consider the possibilities of passive tomography [16], which does not require seismoacoustic sources and estimates the propagation times of signals from the cross-correlation function of the noise field. Long-term seismoacoustic noise measurements on ice carried out within the discussed experiment will be used to investigate this possibility. In this case, we expect broadening of the frequency range of the probing signals to the low-frequency region, as well as a more detailed study of the bottom characteristics at larger depths.

FUNDING

The work was supported by the Russian Foundation for Basic Research (project no. 18-05-70034) and by a grant of the President of the Russian Federation in Support of Leading Scientific schools (no. NSh-5545.2018.5).

REFERENCES

1. V. A. Burov, S. N. Sergeev, A. S. Shurup, and A. V. Shcherbina, *Phys. Wave Phenom.* **21** (2), 152 (2013).
2. T. B. Yanovskaya, *Surface-Wave Tomography for Seismological Researches* (Nauka, St. Petersburg, 2015) [in Russian].
3. A. L. Sobisevich, D. A. Presnov, L. E. Sobisevich, and A. S. Shurup, *Bull. Russ. Acad. Sci.: Phys.* **82** (5), 496 (2018).
4. A. I. Belov and G. N. Kuznetsov, *Acoust. Phys.* **62** (2), 194 (2016).
5. I. V. Gindler and A. R. Kozel'skii, *Akust. Zh.* **38** (1), 29 (1992).
6. A. L. Virovlyanskii, A. Yu. Kazarova, L. Ya. Lyubavin, and A. A. Stromkov, *Acoust. Phys.* **45** (4), 420 (1999).
7. V. V. Goncharov, V. N. Ivanov, O. Yu. Kochetov, B. F. Kuryanov, and A. N. Serebryanyi, *Acoust. Phys.* **58** (5), 562 (2012).
8. V. M. Kudryashov, *Acoust. Phys.* **48** (2), 180 (2002).
9. D. A. Presnov, R. A. Zhostkov, A. S. Shurup, and A. L. Sobisevich, *Bull. Russ. Acad. Sci.: Phys.* **81** (1), 68 (2017).
10. A. L. Sobisevich, D. A. Presnov, V. M. Agafonov, and L. E. Sobisevich, *Seism. Instrum.* **54** (6), 677 (2018).
11. D. A. Presnov, R. A. Zhostkov, V. A. Gusev, and A. S. Shurup, *Acoust. Phys.* **60** (4), 455 (2014).
12. A. V. Kalinin, *Marine Seismic-Acoustic Researches* (Nedra, Moscow, 1983) [in Russian].
13. V. A. Burov, S. N. Sergeev, and A. S. Shurup, *Acoust. Phys.* **53** (6), 698 (2007).
14. D. A. Presnov, A. L. Sobisevich, and A. S. Shurup, *Phys. Wave Phenom.* **24** (3), 249 (2016).
15. A. L. Sobisevich, D. A. Presnov, L. E. Sobisevich, and A. S. Shurup, *Dokl. Earth Sci.* **479** (1), 355 (2018).
16. R. A. Zhostkov, D. A. Presnov, A. S. Shurup, and A. L. Sobisevich, *Bull. Russ. Acad. Sci.: Phys.* **81** (1), 64 (2017).